Characteristics of diabatic heating associated with mesoscale convective systems over Indian Ocean from radiosonde and GPS radio occultation

Khairunisa Febrina[1], Tri Wahyu Hadi[2], Noersomadi[3]

[1] Weather and Climate Prediction Laboratory, Faculty of Earth Science and Technology, Institut Teknologi Bandung, Indonesia
[2] Atmospheric Science Research Group, Faculty of Earth Science and Technology, Institut Teknologi Bandung, Indonesia
[3] Center of Atmospheric Sciences and Technology, National Institute of Aeronautics and Space, Indonesia

E-mail: kfebrina@meteo.itb.ac.id

Abstract. This study aims to investigate the characteristics of diabatic heating profiles associated with appearances of Mesoscale Convective Systems (MCSs) over Sumatra Island (SI) and Indian Ocean (IO) including the transitional offshore zone (TZ). We define the parameters of eccentricity, cloud lifetime, and cloud coverage from Multi-Functional Transport Satellite (MTSAT) infrared imageries to identify the MCSs. We derive the diabatic heating profiles over SI and IO using radiosonde data collected during Cooperative Indian Ocean Experiment on Intraseasonal Variability in the Year 2011 (CINDY2011) / Dynamics of the Madden Julian Oscillation (DYNAMO) campaign. We also estimate the diabatic heating profiles from the GPS Radio Occultation incorporated with the European Centre for Medium-Range Weather Forecasts (ECMWF) reanalysis data over TZ, where the radiosonde observations were limited. The results show that heating occurred throughout the entire troposphere during the mature stages of MCSs with more variations in the amplitude and maximum heating up to 20 K/day overland. Furthermore, the altitude of maximum heating over SI is lower than that of IO and TZ. Over SI and TZ, profiles of dissipations (postmature) stage are characterized by cooling in the lower altitude and an upward shift of maximum heating. By analyzing vertical velocity profiles, we confirm that cooling (heating) processes are associated with updraft (downdraft) in the cloud systems. In addition, the presence of cooling that occurs in layers close to the surface could indicate the formation of cold pool during the dissipation phase of the MCSs.

1. Introduction

Diabatic heating in the atmosphere appears from combination of latent heat released during the phase changes of water substance, convergence of radiative fluxes, and turbulence flux of sensible heat. This type of heating is a source of excitation of atmospheric waves that play important roles in generating and maintaining general-, as well as, local-circulations (e.g., Hartmann et al. [3], Mapes and Houze[14]). Knowledge of the diabatic heating profiles in the atmosphere is fundamental to understand the mechanism of wave generation and propagation, which are crucial information for the development and advancement of weather and climate models.

Mesoscale Convective System (MCS; Houze [7]), is an organized group of thunderstorms that produces a contiguous precipitation area measuring 100 km or more (Houze [7]). The MCS often evolves to form the convective towers at its mature stage, then transforms into convective-stratiform complexes, before further decays into stratiform-rain only. It is well known that convective systems produce significant diabatic heating due to a large amount of water vapor condensation in their development process. Houze [6] pointed out that convective and stratiform regions in MCSs strongly characterize tropospheric heating profiles. Additionally, Yuan and Houze [19] showed that there is high frequency of occurrences of MCSs in the Maritime Continent (MC) especially over the Eastern Indian Ocean (Trismidianto et al. [16]).

Diabatic heating profiles associated with MCSs have been previously studied in several works, as summarized in Table 1. It can be seen that researches on diabatic heating profiles have been mainly conducted over the oceanic environment and outside MC region. It should also be noted that the height of heating peaks vary from place to place and cooling peaks were only observed in some cases. Around MC, results from measurements conducted over the South China Sea (Johnson and Young [11]) and that of the Indian Ocean (Katsumata et al. [12]) show some differences in terms of the height of heating and cooling peaks. These results posed at least two questions. (a) Are heating profiles over MC distinctly different from those of other regions? And (b) what factors determine the height of heating/cooling peaks?

Table 1. Summary of previous research on diabatic heating profiles with information on the height of heating and cooling peaks as highlighted results.

Author(s)	Location	Heating Peak (hPa)	Cooling Peak (hPa)
Reed and Recker (1971)	West Pacific (Close to the island)	450	-
Yanai et al. (1973)	West Pacific including	450	-
	Marshall Island	500	-
Johnson (1976)	Florida (Land)	500	-
Houze (1982)	Atlantic (Sea)	300	600
Johnson and Young (1983)	South China Sea (Close to the Island)	400-300	700
Houze and Rapport (1984)	Atlantic (include Pohnpei Island)	400	800
Johnson and Ciesliski (2000)	Atlantic (Sea)	400	-
Katsumata et al. (2011)	Indian Ocean (Sea)	400	-

The aim of this study is to investigate the characteristics of tropospheric diabatic heating profiles associated with appearances of MCSs over Sumatra Island (SI) and eastern part of Indian Ocean (IO), including the transitional zone (TZ) between those two regions. These studied areas represent a gradual change of the environment, from land, to coastal zones, and open ocean, also from MC region to the area that is close to its perimeter. Thus, this study differs from previous similar research in terms of land-to-ocean coverage. In addition, a novel approach to utilize atmospheric profiles from both radiosonde and GPS Radio Occultation (RO) data for estimation of diabatic heating profiles is herein also highlighted. Detailed description about data and methods is presented and the next section.

2. Data and Methodology

In this research we use geostationary satellites data from the Multi-Functional Transport Satellite (MTSAT-2R), which is operated by the Japan Meteorological Agency (JMA) for identify the MCSs. For obtain the diabatic heating profiles, we use radiosonde data obtained during Cooperative Indian Ocean Experiment on Intraseasonal Variability in the Year 2011 (CINDY2011) / Dynamics of the Madden Julian Oscillation (DYNAMO) as reported in Yoneyama et al. [18]. In addition, we also use the Global Positioning System Radio Occultation (GPS-RO) technique, which is an active limb sounding of the atmosphere and ionosphere from the propagation of GPS signal to the low Earth orbit satellites (Anthes et al. [1]). The COSMIC Data Analysis and Archive Center (CDAAC) website

produced several product data. There are several mission used in this study which is COSMIC wetPrf (Constellation Observing System for Meteorology Ionosphere & Climate), TerraSar-X (The German TerraSar-X mission), and GRACE (Gravity Recovery and Climate Experiment). The continuous GPS-RO observation may provide atmospheric profiles inside the MCSs that can resolve the problem of limited number of radiosonde data. The European Centre for Medium-Range Weather Forecasts (ECMWF, Dee et al [3]) reanalysis data were also incorporated with GPS-RO in TZ and SI where radiosonde observations were insufficient.

The area of this study can be seen in figure 1. We part the area into three sub-regions which is SI, TZ, and IO. The three sub-regions differ not only by location, but also by data usage. Specifically for TZ, we used one radiosonde data retrieved inland combined with GPS-RO; for IO we use sounding data from RV/Mirai combine with the nearest GPS-RO; and for SI we use ground-based sounding data from three stations in Medan, Padang, and Singapore.

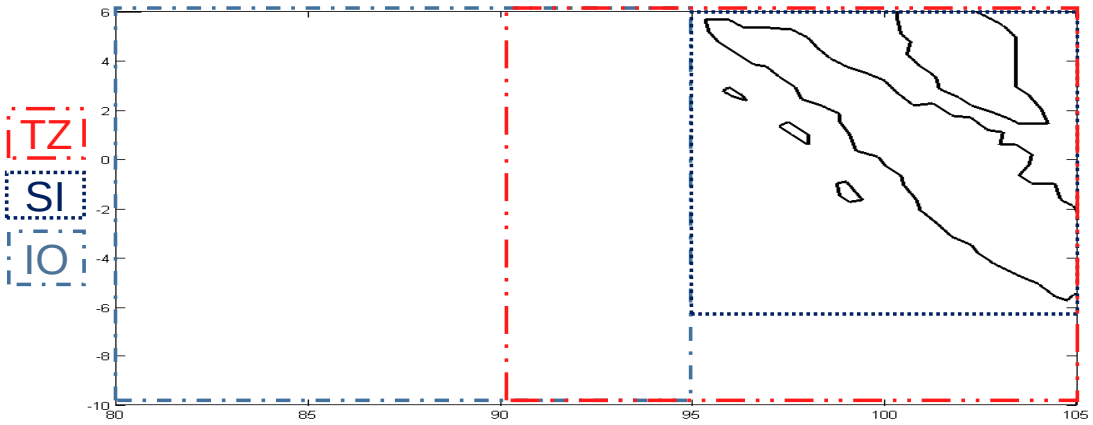

Figure 1. Area of study defined as Sumatra Island (SI; 95°E-105° E,6°N-6°S); Indian Ocean (IO; 78°E-95°E,6°N-10°S) that adjacent to the SI, including the Transitional Zone between those two regions (TZ; 90°E-105°E,6°N-10°S).

To identify the MCS in this study, we use the equivalent Temperature Black Body (hereafter T_{bb}) from the MTSAT-2 infrared imageries for data from 20 November 2011 to 11 December 2011. The satellite data has spatial resolutions 0.05° x 0.05° and at one hour time interval. This study adapts the method of Machado et al. [13] that automated-objectively classified MCSs in satellite images using the criteria as described in table 2 (defined in Jirak et al. [8]). Examples of the observed characteristics are shown in figure 2.

Table 2 MCS definitions based on the analysis of IR satellite imagery adapted from Jirak et al. [8].

MCS category	Size	Duration	Shape
MCC	Cold cloud region ≤ -52°C with an area ≥50 000 km^2	Size definition met for ≥6h	Eccentricity ≥ 0.7 at time of maximum extent
PECS			0.2 ≤ eccentricity < 0.7 at time maximum extent
MβCCS	Cold cloud region ≤ -52°C with an area ≥30 000 km^2 and maximum size must be ≥50 00 km^2	Size definition met for ≥3h	Eccentricity ≥ 0.7 at time of maximum extent
MβECS			0.2 ≤ eccentricity < 0.7 at time maximum extent

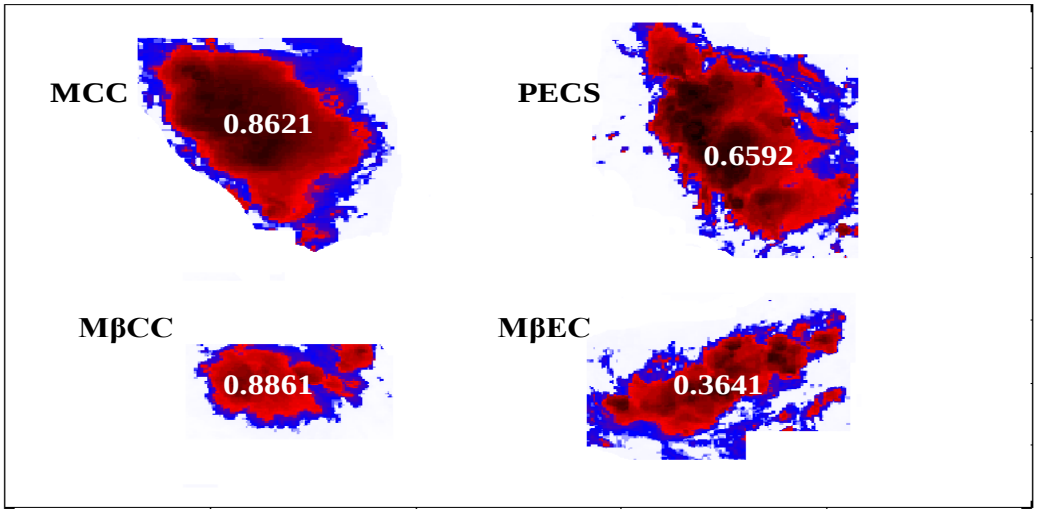

Figure 2. Examples of MCS identification results (with eccentricity determined using Machado method) for four cases of: MCC on November 22nd, 2011 at Sumatera Island, PECS on November 25th, 2011 in the region between Sumatera Island and the Indian Ocean, MβCC on November 20th, 2011 in the Indian Ocean, and MβEC on November 22nd , 2011 at Sumatra Island.

To determine the samples of MCSs for further analyses, we use the information of the appearances of MCS in the three sub-regions and examine coinciding sounding data. Using the radiosonde and GPS-RO temperature profiles, we can calculate the apparent heat source for each sample of MCS. The radiosonde data in SI retrieved from Radiosonde Sounding stations located in Medan (3.565°N, 98.75°E) [21], Padang (0.884°S, 100.35°E) [22], and Singapore (1.33°N , 103.8°E) [20]. Meanwhile, in region IO and TZ we used data from JAMSTEC RV/MIRAI (located within -8°N – 3°N, 78°E – 100°E) [23] and GPS-RO from several missions that match spatially and temporally with the cases of MCS. The spatial distribution of sounding data is illustrated in figure 3. Atmospheric parameters such as meridional wind and zonal wind produced by ECMWF ERA-INTERIM were used to complement GPS-RO data, which only contain temperature and pressure profiles.

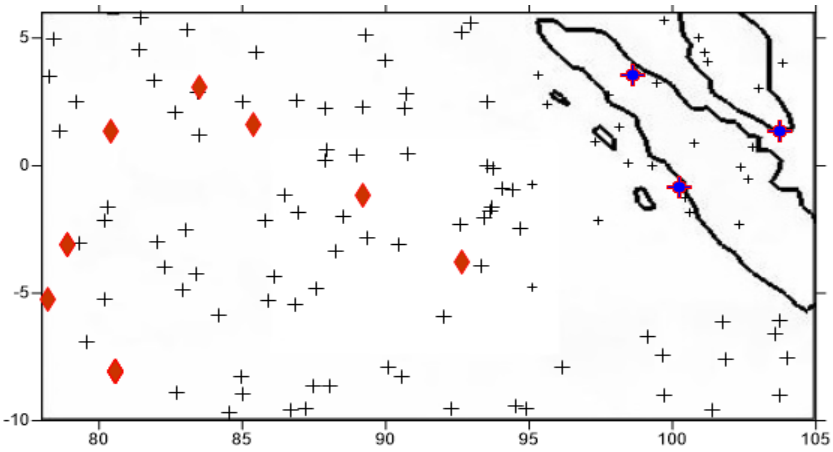

Figure 3. Distribution of GPS-RO data (+), the locations of JAMSTEC RV/MIRAI (♦), and the locations of stations inland (●).

To observationally estimate diabatic heating associated with MCS using upper-air soundings, we use the method of Yanai et al. [17]. Their method is to calculate the apparent heat source Q_1 by adding the horizontal and vertical advection components to the observed temporal variation of dry static energy

(for Q_1). The apparent heating Q_1 of the large-scale motion system consists of the heating due to radiation, the release of latent heat by net condensation, and vertical convergence of the vertical eddy transport of sensible heat, which can be expressed as

$$Q1 \equiv \frac{\partial \bar{s}}{\partial t} + \overline{\boldsymbol{v}}\,\nabla\bar{s} + \frac{\partial \bar{s}\bar{\omega}}{\partial p} \tag{1}$$

In the above, most of the notations are conventional; Q_1 is the apparent heat source (K/day), $\partial\bar{s}(\partial t)^{-1}$ is the dry static energy lapse rate, $\overline{\boldsymbol{v}}\,\nabla\bar{s}$ is the horizontal divergence, $\partial\bar{s}\bar{\omega}(\partial p)^{-1}$ is vertical advection. The horizontal averages are denoted by ($\bar{}$). For calculating the horizontal averages, we used Delaunay Triangulation following that of other research (Reed and Recker [15], Johnson [9], Katsumata et al. [12]). This method need three point locations circumventing an isolated area. For region SI we used observations from stations in Medan, Padang, and Singapore; for region TZ, we used two point locations of GPS-RO mission that coincide with the observation station inland in either Medan or Padang; and for region IO, we used two point locations of GPS-RO mission that are nearest to the RV/MIRAI during its cruise.

The sensible heat budget of the area is taken into account in terms of the dry static energy *s*, defined as the sum of the sensible heat and potential energy per unit mass. That is,

$$s = c_p T + gz \tag{2}$$

where c_p is the specific heat of dry air at constant pressure, *T* temperature, *g* the gravitational acceleration and *z* geopotential height.

The area-averaged horizontal divergence over the triangular region were computed by,

$$\overline{\nabla \cdot V} = \frac{1}{A}\left(\oint u\mathrm{d}y - \oint v\mathrm{d}x\right) \tag{3}$$

where *u* and *v* are the eastward and the northward components of the winds along the periphery of the triangle whose area is denoted by *A*.

The average vertical *p*-velocity is obtained by,

$$\bar{\omega} = \int_{po}^{p} \overline{\nabla \cdot V}\,\mathrm{d}p \tag{4}$$

in which the original estimates of $\overline{\nabla \cdot V}$ were slightly corrected to make $\bar{\omega}$ vanish at 100 mb. All the computations were carried out for certain MCS case in each region and at intervals of 100 mb in pressure level. All the vertical differentiations were replaced by either of these finite differences:

$$f'(x) = (f(x+h) - f(x-h))(h)^{-1} \quad \textit{(Central difference)} \tag{5}$$

$$f'(x) = (f(x+h) - f(x))(h)^{-1} \quad \textit{(Forward difference)} \tag{6}$$

$$f'(x) = (f(x) - f(x-h))(h)^{-1} \quad \textit{(Backward difference)} \tag{7}$$

depending on data availability and reliability.

The Q_1 measures the net heating effects of convective and radiative processes averaged over the area under investigation. Their vertical profiles have been determined in many regions of the tropics and subtropics for convective systems containing both convective-scale (cumulonimbus) and mesoscale components (Yanai et al. [17], Johnson [9]). In the tropics, vertical advection $\partial\bar{s}\bar{\omega}(\partial p)^{-1}$ is dominant in area with size relevant to this study. Therefore, since $\partial\bar{s}(\partial t)^{-1}$ is roughly constant in the tropics, the net heating may be interpreted as a direct indication of the mean vertical motion $\bar{\omega}$ in the area. In this study, we analyze diabatic heating profile associated with MCS in three sub-regions, without discussing further detail on each type of MCS.

3. Results and Discussion

3.1. Convective Activities in the Area of Study

In this section, we first discuss the results of MCS identification from satellite imageries acquired in the period of study, which corresponded to the active phase of Madden-Julian Oscillation (MJO) from 20th November 2011 to 11th December 2011. Basically, the MCS in the Indian Ocean has similar appearance as reported in previous studies (Trismidianto [16]; Yuan and Houze [19]) referring to the definition of MCS from Jirak et al [8]. Figure 4 shows the number of daily occurrences of MCSs that were successfully identified within the area as defined in figure 1. It can be seen from figure 4 that convective activity increased from 20th November 2011 and peaked around 28th November 2011, and then drastically reduced after 2nd December 2011. Results of MCS classification (data not shown) show that more circular type (eccentricity ≥ 0.7) of MCC and MβCC appearances dominated the sample with the total of eight to nine occurrences, while elongated PECS and MβEC occurred only three times. Due to such uneven distribution, we did not differentiate MCS types in the computation of apparent heating profiles.

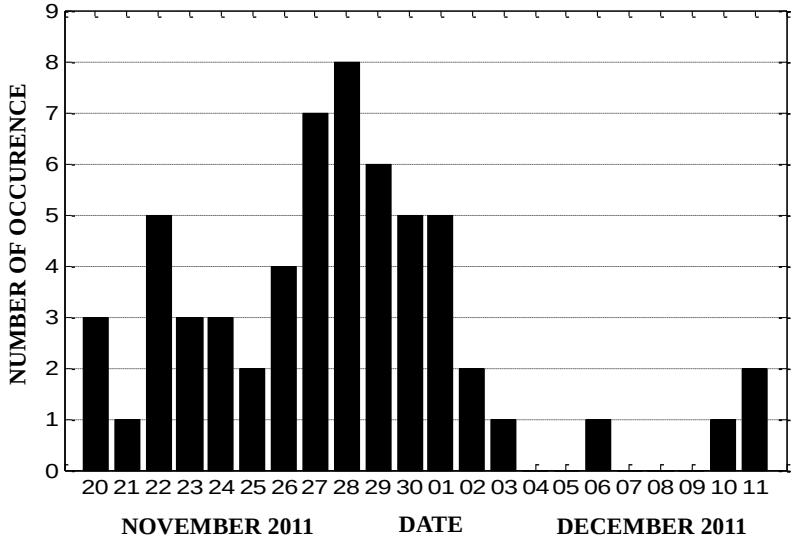

Figure 4. Number of identified MCSs in the area of study (6°N-6°S; 95°E - 105°E) during the period of 20th November to 11th December 2011.

Relatively frequent appearances of MCSs found in this study are consistent with results from previous works. As pointed out by Yuan and Houze [19] and Trismidianto [16], the Eastern Indian Ocean is convectively active region due to very contrast difference between SI and the warm seas of the IO. Such land-sea contrast could trigger strong diurnal cycle leading to the creation of large convective systems like MCS.

3.2. Diabatic Heating Profiles

We computed diabatic heating profiles associated with the appearances of MCS in three sub-regions by methods discussed in Section 2. As previously mentioned, we analyzed the results by grouping the heating profiles according to three sub-regions (SI, TZ, and IO) and two phases of MCSs (mature and dissipation) so that in total we have six groups of samples. Notwithstanding limitation in data availability, we managed to obtain four samples of heating profile for each group as shown in figure 5 and figure 6.

It is clear from figure 5 that, during the mature phase of MCS, warming occurs throughout the troposphere regardless of the sub-regions. This result is consistent with those of Yanai et al. [17],

Johnson [9], Johnson and Young [11], and Katsumata et al. [12]. However, heating profiles over land showed more variations in the amplitude with maximum heating up to 20 K/day, compared to other sub-regions where maximum values are below 20 K/day. Moreover, there are also marked differences in the height of layers where the maximum heating occurs.

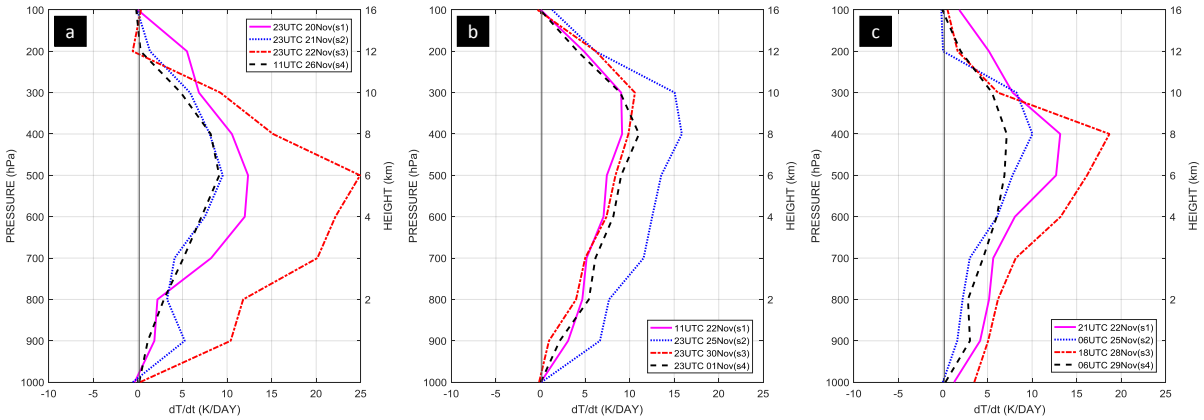

Figure 5. Profiles of diabatic heating computed as apparent heating Q_1 (see text) in three sub-regions of (a) Sumatra Island (SI), (b) Transition Zone (TZ), and (c) Indian Ocean (IO) corresponding to mature phase of MCSs at different times.

Diabatic heating profiles that correspond to dissipation phase of the MCSs (figure 6) show a general pattern, in which negative values (cooling) appear at the lower layers of troposphere between 1000 to 700 hPa. It should also be notable that maximum heating shifts upward to occupy middle and upper troposphere. The upper tropospheric maximum is known primarily to be a consequence of latent heating by condensation and freezing in the anvil, while the cooling in the lower troposphere is largely due to precipitation evaporation and melting (Houze [5]). Moreover, radiative heating and cooling become significant in the stratiform clouds that predominate during the transition phase from mature to dissipation.

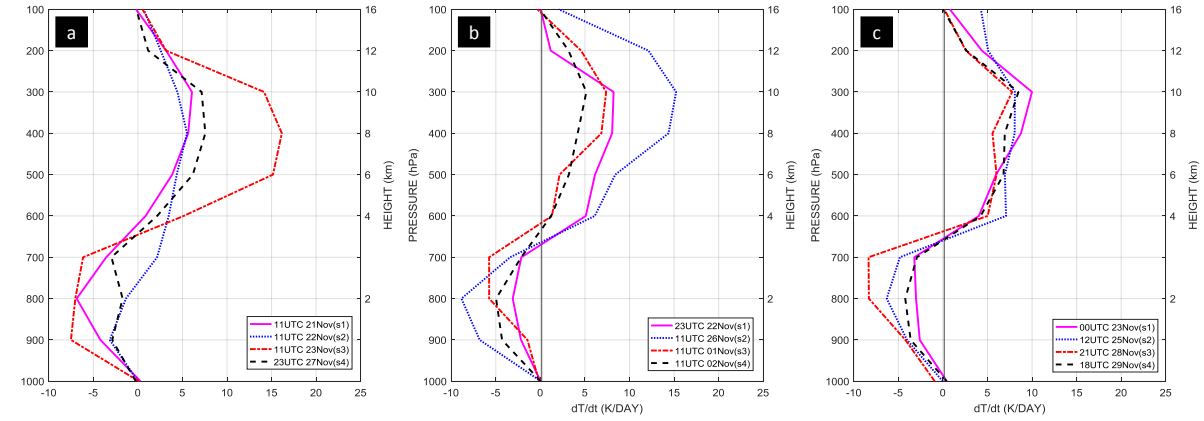

Figure 6. Same as figure 5 but for dissipation phases of MCSs.

Our results confirm that profiles of diabatic heating / cooling due to the presence of MCSs have similar general patterns throughout the MC region. Differences in the amplitude of the heating might be due to several factors such as differences in the atmospheric profile data source (radiosonde, GPS-RO, and reanalysis), the timing between mature and dissipation phases, and the classification of the MCSs.

Herein we restrain from further analysing those factors influencing the amplitude due to insufficient samples. However, differences in the height of heating/cooling peaks seem to be more related to land-sea contrasts.

3.3. Difference in the Height of Heating and Cooling Peaks

In order to see differences in the height of heating/cooling peaks, composite diabatic heating profiles, for the same data groups as in figure 5 and figure 6, are presented in figure 7 and figure 8. It should be clear that for the mature phase, warming peak is centered near 500 hPa for SI, 400-300 hPa for TZ, and 400 hPa for IO. It should be clear that there is a remarkable differences in the height of maximum heating over land and oceans corresponding to the mature phase of MCS. Figure 8 (also figure 5) shows that difference in heating peaks persist during the dissipation phase of MCS, while the height of cooling peaks is almost the same in all sub-regions.

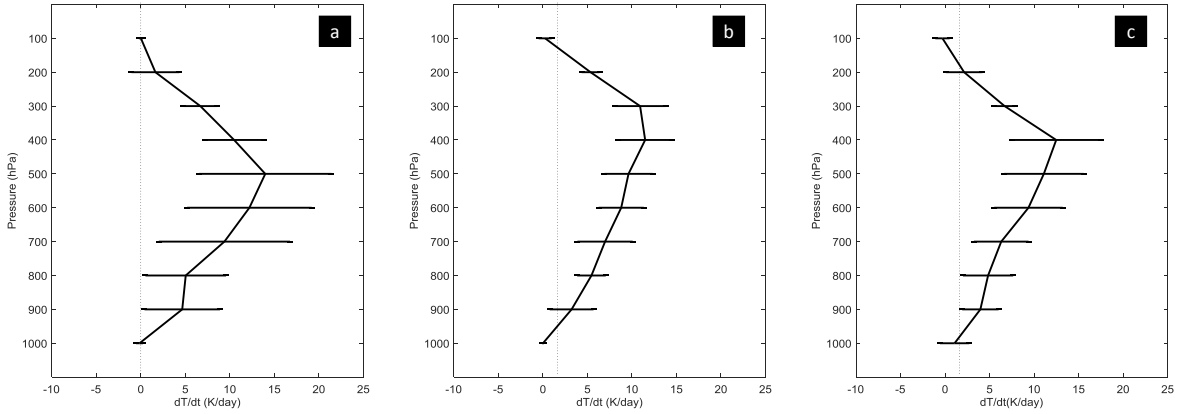

Figure 7. Composite result from the vertical structure of diabatic heating Q1 at the time of maximum / mature for the area a) SI, b) TZ, and c) IO. The horizontal line at each altitude level is the standard deviation calculated from each sample per region

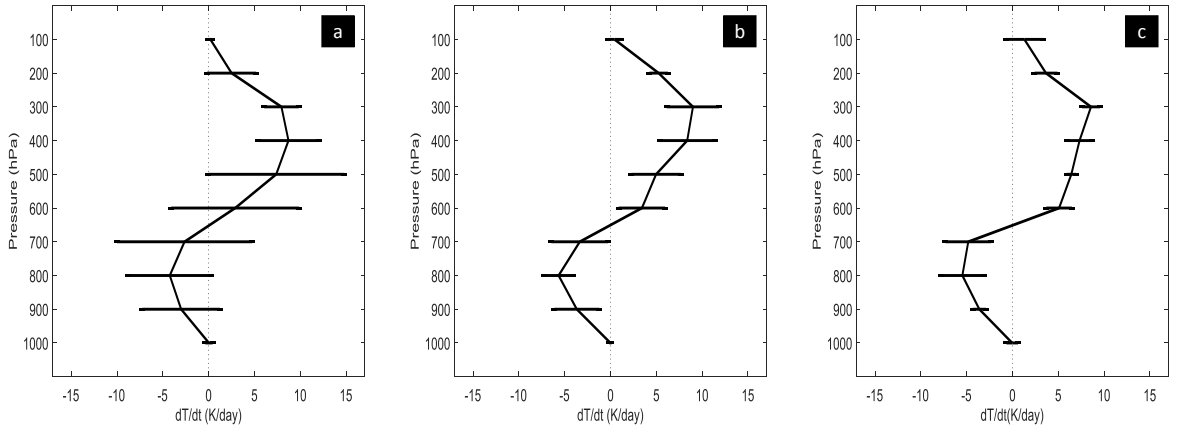

Figure 8. Same as figure 7 but for dissipation phase.

As it has been pointed out in Section 2, the apparent heating Q_1 in the tropics is dominated by vertical advection term. Figure 9 confirms that heating and cooling in the troposphere are in general explained by the occurrence of updrafts and downdrafts. Vertical movement over the ocean is mainly driven by large-scale convergence, whereas topography plays more significant role overland. Sumatra Island can cause strong and rapid development of MCS due to effects of orography and local circulations like

sea/land breezes. The strong updrafts overland transport large amount of water vapor to lower condensation level, because of higher saturation, leading to the release of latent heat that support the development of deeper convention. On the contrary, updrafts over the ocean are normally weaker (see figure 9) causing massive condensation to occur at higher level due to slower rate of vertical moisture transport. This vertical motion pattern is consistent with the result by Cifelli and Rutledge [2].

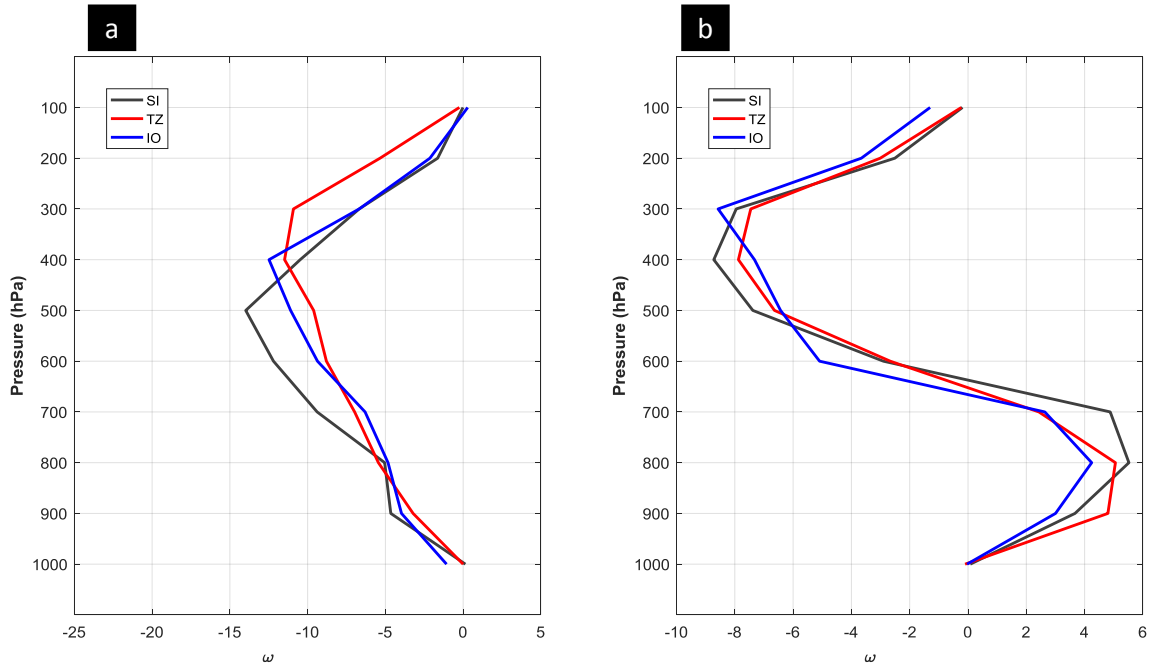

Figure 9. The result of composite vertical motion (ω) of SI, TZ, and IO (see text) in (a) mature phase and (b) dissipation phase.

4. Summary

We investigated the diabatic heating profiles on MCS using data of temperature, pressure, and horizontal wind components obtained from radiosonde observations around the Indian Ocean and the Maritime Continent. We also utilized the temperature profiles retrieved by GPS-RO and the wind data from ECMWF reanalysis to elaborate the characteristics of the diabatic heating over the three different regions of Sumatra Island (SI), Indian Ocean (IO), and the transition zone in between (TZ) during CINDY/DYNAMO campaign periods. In this study, samples of MCSs have been identified from satellite IR imageries using methods suggested by Jirak et al. [8] and diabatic heating profiles were computed following Yanai et al. [18]. A number of 11 MCSs appearances have been identified from the analyzed dataset.

The results show that in all areas (SI, IO, and TZ), during the mature stage of MCSs, heating occurred in the entire troposphere, consistent with the previous study by Yanai et al. [17] and Houze [5][6][7]. However, maximum heating over land is located at the lower altitude compared to that of the oceanic and transitional area. Heating profiles over land also have more variations in the amplitude with maximum value of up to 20 K/day. In the dissipation (postmature) stage, heating profiles of the dissipation stage were characterized by cooling in the lower troposphere and upward shift of maximum heating location for SI and TZ areas, and also sample over IO. The vertical velocity profiles showed that heating and cooling are mainly associated with updraft and downdraft in the cloud systems, this result is similar to the finding by Cifelli and Rutledge [2].

As additional remarks, the presence of cooling that occurs in layers close to the surface could indicate the formation of cold pool. The presence of cold pool may trigger atmospheric instability leading to the development of new convective cells. This result provides supporting evidence for the finding of

Trismidianto et al. [16] about cold pool formation in the dissipation stage of MCS as shown by the diabatic heating profiles. More detailed studies are needed to confirm whether numerical models are able to reproduce correct heating profiles, not only for MCS in general but also for each type MCSs that may appear in MC and Indian Ocean regions.

Acknowledgements
The radiosonde data from CINDY2011/DYNAMO are obtained from the Japan Agency for Marine-Earth Science and Technology (JAMSTEC) (http://www.jamstec.go.jp/iorgc/cindy) and Earth Observing Laboratory (EOL) of UCAR. GPS-RO data are provided by COSMIC Data Analysis and Archive Center (CDAAC) (http://cdaac-www.cosmic.ucar.edu/ cdaac/products.html). The author (KF) is grateful to the organizer of 1st International Conference on Maritime Sciences and Advanced Technology for providing the support.

References

[1] Anthes R A, Bernhardt P A, Chen Y, Cucurull L, Dymond K F, Ector D, Healy S B, Ho S, Hunt D C, Kuo Y, Liu H, Manning K, McCormick C, Meehan T K, Randel W J, Rocken C, Schreiner W S, Sokolovskiy S V, Syndergaard S, Thompson D C, Trenberth K E, Wee T, Yen N L and Zeng Z 2008 The COSMIC/FORMOSAT-3 Mission: Early Results *Bull. Amer. Meteor. Soc.,* **89**, 313–4.

[2] Cifelli R and Rutledge S A 1994 Vertical Motion Structure in Maritime continent mesoscale Convective Systems: Results from a 50-MHz Profiler. *J. Atmos. Sci.,* **51**, 2631–52

[3] Dee D P, Uppala S M, Simmons A J, Berrisford P, Poli P, Kobayashi S, Andrae U, Balmaseda M A, Balsamo G, Bauer P, Bechtold P, Beljaars A C M, van de Berg L, Bidlot J, Bormann N, Delsol C, Dragani R, Fuentes M, Geer A J, Haimberger L, Healy S B, Hersbach H, Hólm E V, Isaksen L, Kållberg P, Köhler M, Matricardi M, McNally A P, Monge-Sanz B M, Morcrette J -J, Park B -K, Peubey C, de Rosnay P, Tavolato C, Thépaut J -N and Vitart F 2011 The ERA-Interim reanalysis: configuration and performance of the data assimilation system *Quarterly Journal of the Royal Meteorological Society* **137** 553–597.

[4] Hartmann D L, Hendon H H and Houze R A Jr 1984 Some implications of the mesoscale circulations in tropical cloud clusters for large-scale dynamics and climate *J Atmos Sci* **41** 113–21.

[5] Houze R A 1982 Cloud clusters and large-scale vertical motion in the tropics *J Meteorology Society Japan* **60** 396–410.

[6] Houze R A 1989 Observed Structure of Mesoscale Convective Systems and implications for Large-Scale Heating *Quaterly Jurnal of The Royal Meteorological Society* **115** 425-61.

[7] Houze R A Jr 2004 Mesoscale Convective Systems *Rev. Geophys* **42**

[8] Jirak I L, Cotton W R, McAnnelly R L 2003 Satellite and radar survey of mesoscale convective system development *Monthly Weather Review* **131** 2428–49

[9] Johnson R H 1984 Partitioning tropical heat and moisture budgets into cumulus and mesoscale components: Implications for cumulus parameterization *Monthly Weather Review* **112** 1590–601

[10] Johnson R H and Ciesielski P E 2000 Rainfall and radiative heating rate estimates from TOGA COARE atmospheric budgets *J Atmos Sci* **57** 1497–514

[11] Johnson R H and Young G S 1983 Heat and moisture budgets of tropical mesoscale anvil clouds *Journal of Atmospheric Scientics* **40** 2138–47

[12] Katsumata M, Ciesielski P E, Johnson R H 2011 Evaluation of budget analyses during MISMO *Journal of Applied Meteorology and Climatology* **50** 241–54.

[13] Machado L A T, Rossow W B, Guedes R L and Walker A W 1998 Life cycle variations of mesoscale convective systems over the Americas. *Mon. Wea. Rev.,* **126** 1630–54.

[14] Mapes B E and Houze R A 1995 Diabatic divergence profiles in western Pacific Mesoscale convective systems *J Atmos Sci* **52** 1807–28.

[15] Reed R J and Recker E E 1971 Structure and properties of synoptic-scale wave disturbances in the equatorial western Pacific *J Atmos Sci* **28** 1117–33.
[16] Trismidianto, Yulihastin E, Satyawardhana H, Nugroho J T and Ishida S 2017 The Contribution of the Mesoscale Convective Complexes (MCCs) to total rainfall over Indonesian Maritime Continent *IOP Conf. Ser.: Earth Environ. Sci* **54** *012027*
[17] Yanai M, Esbensen S and Chu J 1973 Determination of bulk properties of tropical cloud clusters from large-scale heat and moisture budgets *Journal Atmospheric Science* **30** 611–27.
[18] Yoneyama K, Zhang C and Long C N 2013 Tracking pulses of the Madden-Julian Oscilation *Bull. Amer. Meteor. Soc.,* **94** 1971–91
[19] Yuan J and Houze R A Jr 2010 Global Variability of Mesoscale Convective System Anvil Structure From A-Train Satellite Data *Journal of Climate* **21** 5864–88.
[20] UCAR/NCAR - Earth Observing Laboratory. 2012. Singapore Radiosonde L3 Data. Version 1.0. UCAR/NCAR - Earth Observing Laboratory. https://data.eol.ucar.edu/dataset/347.030. Accessed 25 Aug 2017.
[21] Yoneyama, K., Japan Agency for Marine-Earth Science and Technology (JAMSTEC). 2012. Indonesia Site - Medan Radiosonde L3.0 Data. Version 1.0. UCAR/NCAR - Earth Observing Laboratory. https://data.eol.ucar.edu/dataset/347.053.
[22] Yoneyama, K., Japan Agency for Marine-Earth Science and Technology (JAMSTEC). 2012. Indonesia Site - Padang Radiosonde L3.0 Data. Version 1.0. UCAR/NCAR - Earth Observing Laboratory. https://data.eol.ucar.edu/dataset/347.097.
[23] UCAR/NCAR - Earth Observing Laboratory. 2012. R/V Mirai Radiosonde L3.0 Data (ESC Format). Version 1.0. UCAR/NCAR - Earth Observing Laboratory. https://data.eol.ucar.edu/dataset/347.014.